Studies of periodic ferroelectric domains in $KTiOPO_4$ using high-resolution x-ray scattering and diffraction imaging

Z. W. Hu* and P. A. Thomas
Department of Physics, University of Warwick, Coventry CV4 7AL, United Kingdom

W. P. Risk
IBM Corporation Research Division, Almaden Research Center, San Jose, California 95120

(Received 17 February 1999)

A periodically domain-inverted $KTiOPO_4$ crystal, in which inverted ferroelectric domains were produced by electric-field poling, has been studied using high-resolution x-ray scattering and diffraction imaging techniques. The degree of perfection of domain inversion as well as the periodic structure has been revealed in high-spatial-resolution images, and the periodic contrast is shown to arise largely from lattice distortions produced in the poled regions. The $q_{\|}$ dependence of intensity scattered from the domain-inverted structure can be described by a two-component line shape, one with a sharp nearly-pure-Gaussian line, the other with a broad pseudo-Voigt-function profile. A high-angular-resolution method has been combined to elucidate the origin of the two-component profile. The diffuse scattering of the crystal truncation rod along $q_{\perp}$ is observed to follow a power law $q_{\perp}^{-\gamma}$ with $\gamma \sim 2.29 \pm 0.03$ after poling compared with an average value of 2.05 ± 0.03 before poling. Discussions of the electric-field poling and its consequence for the domain-inverted structure are presented in terms of the results of x-ray measurements. [S0163-1829(99)09921-X]

I. INTRODUCTION

There is increasing interest in the fabrication of periodically domain-inverted (PDI) structures in ferroelectric materials because of their novel applications in nonlinear optics[1,2] and acoustics.[3] Macroscopic physical properties of PDI materials and performance of PDI array-based devices rely directly upon how well ferroelectric domains are sequentially inverted via displacements of ions of the structure driven by an external field. To take full advantage of these PDI structures for optical and acoustic devices, it is of considerable importance to establish a fundamental understanding of periodic domain inversion to the same degree as we have for semiconductor layer structures.

Several methods have been used to examine antiparallel ferroelectric domains including chemical etching, x-ray topography,[4–8] physical-property-based measurements,[9–11] scanning electron microscopy (SEM),[12] and atomic force microscopy.[13] Most recently, PDI structures in ferroelectric crystals of $LiNbO_3$ and $LiTaO_3$ have been successfully characterized by x-ray topography,[14,15] phase-contrast imaging,[16] environmental SEM,[17] and scanning-tip microwave near-field microscopy.[18] Here we apply combined high-resolution x-ray scattering and imaging techniques to structural characterization of PDI arrays in $KTiOPO_4$ (KTP), one of the most important and attractive ferroelectric nonlinear optical materials for periodic domain-inversion engineering.[19–21] Compared with other means, the x-ray techniques used in reflection geometry from a PDI crystal or device have the advantages that a crystal is nondestructively examined in an intact format and that PDI arrays are unaffected by the investigation unlike the SEM case where PDI structures are easily altered as a consequence of the electron charge built up on a crystal surface exposed to electron beams.[12] Furthermore, high-resolution x-ray imaging and scattering techniques are highly sensitive to structural deviations from perfection, which allows the lateral domain structure to be imaged and the degree of imperfections to be quantified while little is currently known on a detailed microscopic scale concerning structural perfection of PDI arrays. In the present paper, we report the results of high-resolution x-ray scattering line-shape measurements of a PDI KTP crystal combined with high-spatial-resolution and high-angular-resolution diffraction imaging, in which lateral and in-depth structural details of the PDI arrays are obtained.

II. EXPERIMENTAL DETAILS

A 1-mm-thick *c*-cut section of optical grade hydrothermally grown KTP was used for this study. $\pm c$ faces were determined using x-ray anomalous-scattering diffraction and topography as described in Ref. 6. Then, a 1000-Å-thick aluminum film was deposited on the $+c$ face and patterned using standard lithographic and etching techniques to produce a grating with a period of 24 μm and a duty cycle of about 50:50. The grating was covered with a 2-μm-thick photoresist to protect the grating while etching away the extraneous aluminum. A Cr/Au uniform electrode was applied to the $+c$ side of the crystal. Periodic domain inversion was achieved by repeatedly applying a number of pulses with high voltages varying from 2.0 to 4.5 kV. The grating was removed after the poling process. A high-resolution x-ray diffractometer,[22] which combines a two-crystal four-reflection Ge (220) monochromator with a channel-cut triple-bounce Ge (220) analyzer (Fig. 1), was employed to measure diffraction profiles and maps, using Cu $K\alpha_1$ radiation. The output beam from the monochromator gives an angular divergence of a 10″ arc in the horizontal scattering plane. The real instrumental broadening caused after the analyzer is

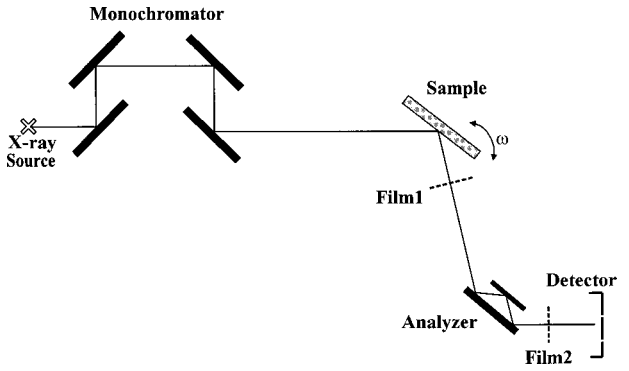

FIG. 1. A schematic diagram of the high-resolution multiple-crystal multiple-reflection diffractometer.

a 5.6″ arc or less in both the ω ($q_{\parallel}$) and ω/θ ($q_{\perp}$) direction for the measured reflection of 004. The instrumental functions follow Gaussian fits. High-spatial-resolution and high-angular-resolution diffraction images were taken, respectively, using two different imaging modes.[14,23] In mode 1, a film was placed before the analyzer and close to the sample so that 1 μm or better spatial resolution is obtainable in the horizontal scattering plane. For mode 2, the film is positioned after the analyzer that defines angular resolution optically. In this mode, the probe becomes sufficiently small in reciprocal space to allow diffuse scattering regions of interest to be pinpointed by high-angular-resolution images.[24–26] Diffraction images were recorded on 25-μm Ilford L4 nuclear emulsion plates.

III. RESULTS AND DISCUSSIONS

Figures 2(a) and 2(b) are high-spatial-resolution diffraction images of the periodically domain-inverted structure in KTP taken on the Bragg peak of the $8\,0\,\overline{8}$ reflection using mode 1. The left side of Fig. 2(a), i.e., the area with rather uniform contrast, corresponds to an untouched region. Periodic black stripes are inverted domains with respect to the original domains, i.e., the periodic gray stripes. The diffraction image in Fig. 2(b) corresponds to a domain-inverted region different from that in Fig. 2(a). An intensity variation arising from dislocations in the middle part of Fig. 2(b) dominates the relatively weak contrast of the domains. Careful inspection shows that there exists a fluctuation in the width of the individual domain images along the grating direction even in the relatively perfect regions. This is a consequence of varying fringing fields present at the edges of the grating electrode.

Sets of diffraction images were taken by the choice of appropriate reflections to investigate the origin of the periodic contrast. An example is given in Figs. 3(a) and 3(b), where the periodically domain-inverted structure is clearly shown in the $2\,0\,\overline{9}$ and $2\,0\,\overline{10}$ topographs. If the periodic contrast originated primarily from anomalous scattering, then the periodic features should be invisible in the $2\,0\,\overline{9}$ topograph as demonstrated in the study of naturally occurring inversion domains in KTP.[6] Hu, Thomas, and Huang[6] have successfully observed the naturally occurring inversion domains in KTP using anomalous scattering, and have shown that the experimentally observed changes in the diffraction

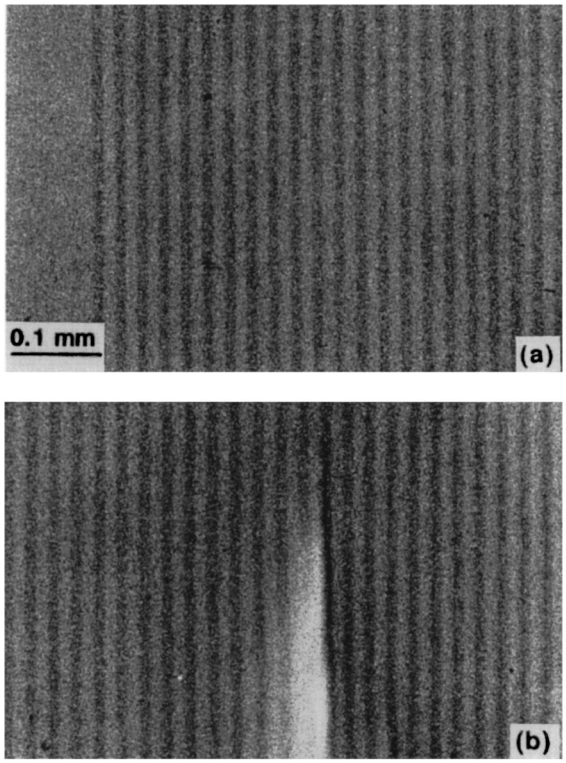

FIG. 2. High-spatial-resolution diffraction images of periodically domain-inverted structure in KTP, $8\,0\,\overline{8}$. (a) A relatively perfect domain-inverted region; (b) a defective region.

contrast of the naturally occurring inversion domains with different reflections are consistent with those predicted by the calculated values of $(|F_{hkl}|^2/|F_{hkl}|^2)$. In the present case, no such systematic changes in the contrast of the artificially domain-inverted structure with different reflections have been observed in the topographs. Therefore, the diffraction contrast is caused largely by lattice distortions produced in the domain-inverted surface regions rather than by anomalous scattering. Considering that the intrinsic rocking-curve widths of the reflections such as $2\,0\,\overline{9}$, $2\,0\,\overline{10}$, and $8\,0\,\overline{8}$ are extremely narrow, less than 1″ arc,[27] the diffraction images of the domains and domain walls are primarily of effective misorientation and extinction contrast. The widths and details of the periodic contrast vary with different angular positions of the probe on the rocking curves. It appears that the PDI KTP domain walls are less well defined than PDI $LiNbO_3$ (LN) domain walls[14] in the x-ray images taken at Bragg-peak positions. This may relate to differences in structural characteristics and poling conditions between KTP and LN. From a structural point of view, the atomic mismatch across the inversion domain walls of KTP would be more readily accommodated than that of LN because of the presence of large ''hole sites'' [28] equivalent to the K sites in the structure and the more deformable nature of the KTP framework compared with the three-dimensional preovskitelike framework of LN.[14]

Rocking-curve measurements have shown that the electric-field poling does not result in appreciable broadening of rocking curves. This has contrasted with the case of a PDI KTP crystal poled by electron-beam bombardment where the 004 rocking-curve width was broadened significantly by

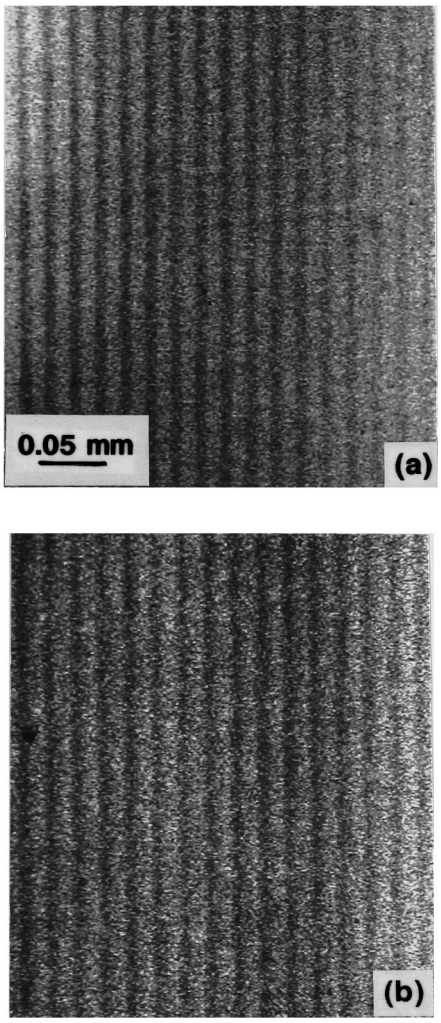

FIG. 3. High-spatial-resolution diffraction images taken with the reflections of (a) $2\,0\,\overline{9}$, and (b) $2\,0\,\overline{10}$. Note that periodic stripes are visible in both (a) and (b).

poling and the subsequent thermal domain-selective etching.[29] Two representative rocking curves of the 0 0 4 reflection measured before and after poling are shown in Fig. 4. The full width at half maximum (FWHM) from the original KTP sample is a 9.7″ arc that is essentially monochromator limited whereas the FWHM of the 0 0 4 reflection obtained from the domain-inverted regions is a 10.4″ arc for the scattering plane normal to the domain walls. It is seen that a major difference between the solid and dotted curves (Fig. 4) lies in the shape of the wings close to the tails. That is, the intensity scattered from the domain-inverted region becomes rather asymmetric, being swollen on the high-angle side. Transverse ($q_{\parallel}$) and longitudinal ($q_{\perp}$) scans, which are parallel and perpendicular to the crystal surface, respectively, were then measured using the triple-bounce analyzer to examine the detailed structural information. Because of the lattice distortions produced by poling, it is more appropriate to analyze integrated $q_{\parallel}$-scattering and $q_{\perp}$-scattering profiles. These are obtained by integrating over $q_{\perp}$ and $q_{\parallel}$ from the reciprocal-space data. The intensity of scattering as a function of $q_{\parallel}$ close to the $0\,0\,\overline{4}$ reflection, integrated over $q_{\perp}$, before and after poling is given in Figs. 5(a) and 5(b). The best description of the wave-vector dependence of intensity scattered from the domain-inverted region is found using a pseudo-Voigt function,[30] which can be written as

$$I_{(q)} = I_0 \left\{ \eta \frac{2}{\pi} \frac{w}{4(q-q_c)^2 + w^2} + (1-\eta)\sqrt{4/\pi} w \times \exp\left[-\frac{4}{w^2}(q-q_c)^2 \right] \right\}, \quad (1)$$

where I_0 is the amplitude, q_c is the center, w is the FWHM, and η is the Lorentzian fraction or the line-shape factor. The $q_{\parallel}$ dependence of intensity scattered from the original crystal can be described well by a pure Gaussian fit [Fig. 5(a)], whereas the $q_{\parallel}$-peak shape after poling [Fig. 5(b)] was distorted such that the peak was split into two components ($\Delta q = 6.7 \times 10^{-5}\,\text{Å}^{-1}$), one having $\eta = 0.08$, the other giving $\eta = 0.47$.

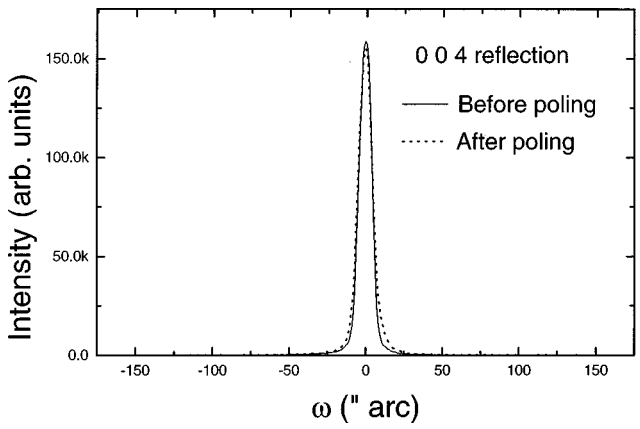

FIG. 4. Rocking curves of the $0\,0\,\overline{4}$ reflection measured before and after poling.

Figure 6(a), a high-angular-resolution image taken using mode 2 at the $q_{\parallel} = 0.000\,19\,\text{Å}^{-1}$ position that is on the high-angular or component-2 side [Fig. 5(b)], shows that intense contrast only emerges in a defective part of the domain-inverted crystal. The contrast of the small region is reversed in Fig. 6(b), the diffuse-scattering topograph that was taken at the $q_{\parallel} = -0.0004\,(\text{Å}^{-1})$ position, i.e., on the low-angular side [Fig. 5(b)]. This suggests that component 1 emanates largely from the main part of the treated region, which is of a comparable perfection to the untreated crystal in terms of the width of the diffraction profile. However, component 2 emanates primarily from the small defective part of the treated region, i.e., the dark area in Fig. 6(a). There are essentially two contributions to the width of the diffraction profile, i.e., the distribution of lattice tilts and the lateral correlation length. The contribution of the tilt distribution to the diffraction profile has been accounted for by the separation of the profile into components 1 and 2; therefore we are now able to obtain the lateral correlation length from the $q_{\parallel}$ scans. Component 1 corresponds to a lateral correlation length of $\sim 7.8\ \mu$m, the same value as that obtained from the original crystal whereas component 2 gives a lateral correlation length of 4.8 μm, i.e., the average size of mosaic blocks in the defective region. An increase in the diffusely-scattered intensity after domain-inversion processing is illustrated in Fig. 5(c). The diffuse-scattering images show that the stron-

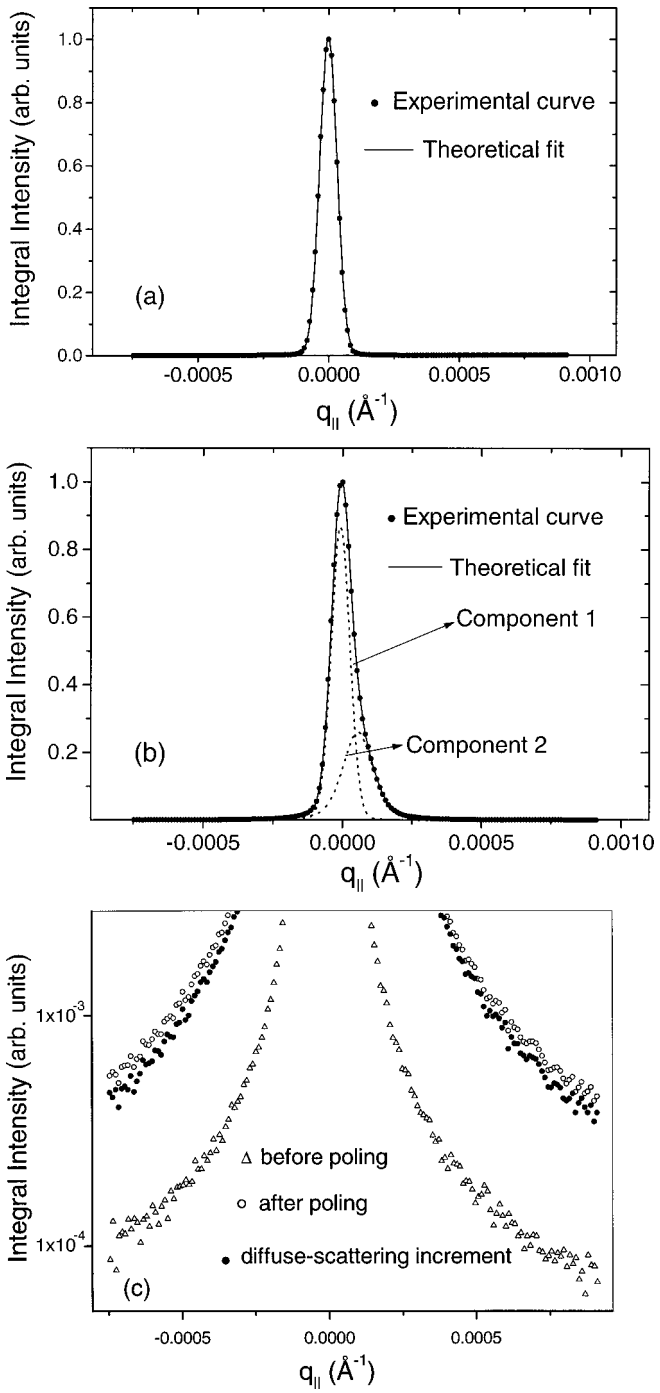

FIG. 5. The integral intensity of scattering as a function of $q_{\parallel}$ measured before poling (a) and after poling (b) for $(0,0,\bar{4}+q_{\parallel})$. The scattering plane is normal to the domain walls. (c) illustrates an increase in the diffusely scattered intensity along $q_{\parallel}$ after poling.

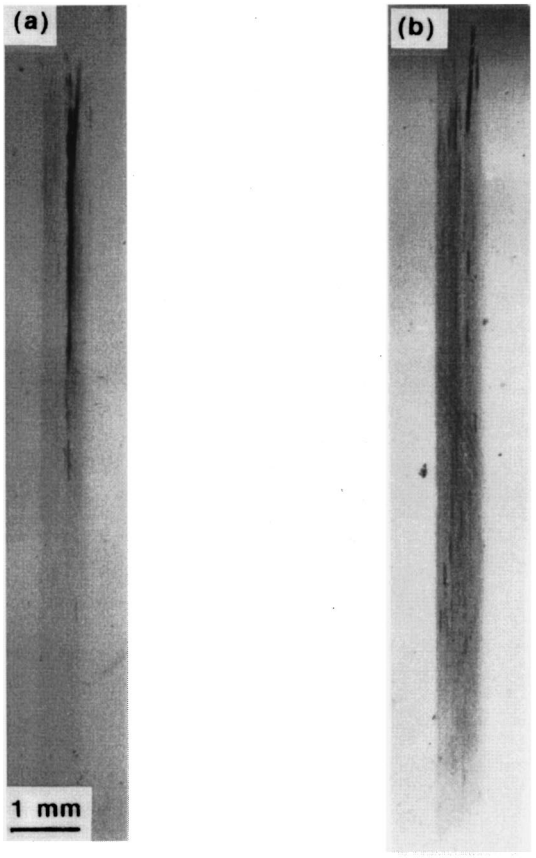

FIG. 6. High-angular-resolution images taken at (a) $q_{\parallel}=0.000\,19\,\text{Å}^{-1}$ in Fig. 5(b), and (b) $q_{\parallel}=-0.000\,4\,\text{Å}^{-1}$ in Fig. 5(b).

gest contribution to diffuse scattering comes from dislocations, which appear as black lines in Fig. 6(b). But it is noted that the integrated diffusely scattered intensity is the mixed effect of the dislocations, the domain walls, mosaics, and point defects.

The $q_{\perp}$ dependence of intensity scattered from the original and domain-inverted crystals, the inset of Fig. 7, shows the same functional form with the same FWHM. The best fit to the $q_{\perp}$ diffraction profiles gives $\eta=0.18$ before poling and $\eta=0.16$ after poling. The diffuse-scattering streak along $q_{\perp}$ or $q_{[00\bar{1}]}$ is the crystal truncation rod (CTR) that arises from the abrupt termination of the crystal surface.[31,32] The scattering of the CTR is highly sensitive to the structure and roughness of surface or interface.[31–33] The intensity scattered from both the original crystal surface and the domain-inverted surface (Fig. 7) is found to follow a power law, i.e., $I(q_{\perp}) \sim q_{\perp}^{-\gamma}$ in the range $q_{\perp} \geqslant 4.80\times10^{-4}\,\text{Å}^{-1}$. The original crys-

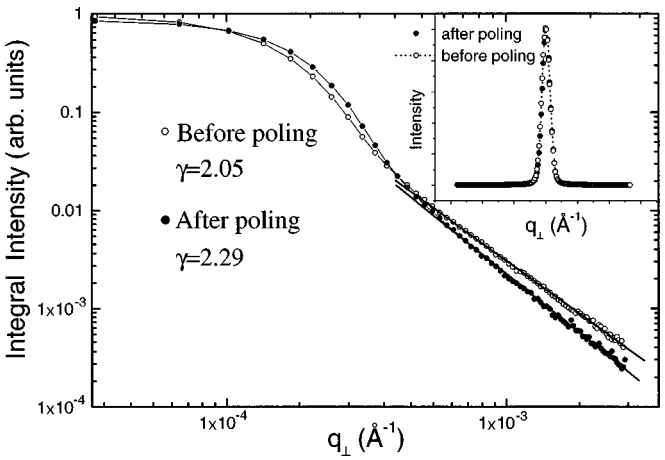

FIG. 7. The intensity of scattering, integrated over $q_{\parallel}$, as a function of $q_{\perp}$ measured before and after poling for $(0,0,\bar{4}+q_{\perp})$. The solid lines represent the power-law fits. The inset displays that the poling does not change the functional form of the $q_{\perp}$ dependence of intensity.

tal surface has a power γ of 2.05 ± 0.03, which corresponds to a smooth surface $\gamma=2$ predicted by dynamic theory[34] and the theory of the CTR.[31,32] The power of γ has increased to 2.29 ± 0.03 after poling. It seems that this feature does not change with different azimuthal angles such that the scattering plane is normal and parallel to the domain walls, respectively.

The diffraction and scattering results indicate that the crystal has been both structurally and microstructurally altered, to some extent, by introduction of periodic inversion domains. Periodic domain inversion is a kinetic process in which the cations and anions of the structure are rapidly displaced by high-voltage pulses applied on the crystal surfaces such that the resulting spontaneous polarization in the poled regions is reversed with respect to the rest of the original crystal. Electric-field-induced and ion-movement-related strain fields take place accompanying nucleation and growth of new inversion domains on the crystal surface. Strain fields induced by the electric field include both the converse piezoelectric term and the electrostrictive term because of the high electric-field strength applied and the local fields developed on the crystal surface. The piezoelectric strain has an opposite sign (expansion/contraction) between neighboring inverted and uninverted domains, and varies with different regions because of a variation of the local electric fields.[35] The components of the instantaneous piezoelectric strain produced on the crystal surface by the external field are calculated to be $S_{11}=\pm7.64\times10^{-6}$, $S_{22}=\pm2.22\times10^{-5}$, and $S_{33}=\pm5.16\times10^{-5}$ for the applied electric-field strength of 2.0 kV/mm ($\pm$ signs correspond to the inverted and uninverted domains, respectively). The electrostrictive term has the same sign in both the inverted and uninverted domains, unlike the converse piezoelectric strain in this respect. The resulting electric-field-induced strains are, therefore, not equal on average in the absolute value between the inverted and uninverted domains, which gives rise to an extra distortion at the domain front. The ion-movement-related strain is produced by the drastic displacements of the ions activated by the high electric field. The K ions undergo displacements of 0.1641, -0.1305, and 1.507 Å along [100], [010], and [001], respectively, for domain inversion. The highly distorted TiO_6/PO_4 framework is forced to adjust accordingly in reversing the sense of the spontaneous polarization.[28] It is seen that the ion-movement-related strain is inseparable from that induced by the local electric fields. These domain-inversion related strains interact with initial strain fields present in the crystal such that the number of defects typically rises, and therefore the degree of lattice tilts increases in some more defective regions. This may explain why the asymmetric $q_\parallel$-scattering profile is observed in the domain-inverted crystal. Furthermore, the increase in the power of γ in the power law, $I(q_\perp)\sim q_\perp^{-\gamma}$, is related to the lattice distortions induced during domain inversion. As seen above, the domain-inversion-induced distortions decrease with increasing depth largely because of the field decay towards deeper parts of the crystal. The depth dependence of the lattice distortions produced close to the crystal surface results in a variation in the electron density $\rho(z)$ along the z direction. Assuming the electron density varies as a function of z^α, then we have the power $\gamma=2+2\alpha$ according to Ref. 31. The value of α is ~0.14 for the domain-inverted KTP surface.

IV. CONCLUDING REMARKS

We have carried out high-resolution measurements of the x-ray diffraction line shape and CTR scattering from a PDI structure in KTP. Combined with diffraction-imaging techniques, we have been able to observe and quantify the structural details of the PDI arrays that would be unobtainable by other nondestructive characterization techniques while these structural properties play an important role in determining device performance.[36] The present work indicates that the origin of the contrast of the artificially domain-inverted structure is, to some extent, different from that of the naturally occurring inversion domains[6] in reflection topographs. The high-resolution $q_\perp$-scattering measurements indicate that the crystal surface roughens because of lattice distortions induced near the crystal surface as a result of domain-inversion processing. Furthermore, the observation of the two-component line shape of the $q_\parallel$ dependence of intensity has shown a variation of the degree of perfection of the crystal in the domain-inverted regions. It should be noted that the conversion efficiency experimentally achieved from the KTP sample is lower than the theoretically predicted value, and the output power from the different poled regions is not strictly uniform. Hence, this is consistent with the results of x-ray diffraction measurements that provide a structural understanding of periodic domain inversion and the poorer optical performance.

ACKNOWLEDGMENT

This work was supported by the UK EPSRC under Grant No. GR/K92955.

*Present address: Universities Space Research Association (USRA), 4950 Corporate Drive, Suite 100, Huntsville, AL 35805.

[1] J. Armstrong, N. Bloembergen, J. Ducuing, and P. S. Pershan, Phys. Rev. **127**, 1918 (1962).
[2] M. M. Fejer, Phys. Today **47** (5), 25 (1994).
[3] Y. F. Chen, S. N. Zhu, Y. Y. Zhu, and N. B. Ming, Appl. Phys. Lett. **70**, 592 (1997).
[4] T. Vreeland and V. S. Speriosu, in *Applications of X-Ray Topographic Methods to Materials Science*, edited by S. Weissmann, F. Balibar, and J.-F. Petroff (Plenum, New York, 1985), p. 501.
[5] H. Klapper, Prog. Cryst. Growth Charact. **14**, 367 (1987).
[6] Z. W. Hu, P. A. Thomas, and P. Q. Huang, Phys. Rev. B **56**, 8559 (1997).
[7] S. S. Jiang, Z. W. Hu, P. Yang, D. Feng, J. Y. Zhao, and J. H. Jiang, Ferroelectrics **140**, 719 (1993).
[8] P. Rejmánková, J. Baruchel, P. Villeval, and C. Saunal, J. Cryst. Growth **180**, 85 (1997).
[9] J. D. Bierlein and F. Ahmed, Appl. Phys. Lett. **51**, 1322 (1987).
[10] G. M. Loiacono and F. A. Stolzenberger, Appl. Phys. Lett. **53**, 1498 (1988).
[11] F. Laurell, M. G. Roelofs, W. Bindloss, H. Hsiung, A. Suna, and J. D. Bierlein, J. Appl. Phys. **71**, 4664 (1992).
[12] R. Le Bihan, Ferroelectrics **97**, 19 (1989).
[13] R. Lüthi, H. Haefke, P. Grütter, H. J. Güntherod, L. Szczesniak, and K. P. Meyer, Surf. Sci. **285**, L498 (1993).
[14] Z. W. Hu, P. A. Thomas, and J. Webjörn, J. Appl. Crystallogr. **29**,

279 (1996).
[15] P. Rejmánková, J. Baruchel, P. Moretti, M. Arbore, M. Fejer, and G. Foulon, J. Appl. Crystallogr. **31**, 106 (1998).
[16] Z. W. Hu, P. A. Thomas, A. Snigirev, I. Snigireva, A. Souvorov, P. G. R. Smith, G. W. Ross, and S. Teat, Nature (London) **392**, 690 (1998).
[17] S. N. Zhu and W. W. Cao, Phys. Rev. Lett. **29**, 2558 (1997).
[18] Y. L. Lu, T. Wei, F. Duewer, Y. Q. Lu, N. B. Ming, P. G. Schultz, and X. D. Xiang, Science **276**, 2004 (1997).
[19] M. C. Gupta, W. P. Risk, A. C. G. Nutt, and S. D. Lau, Appl. Phys. Lett. **63**, 1167 (1993).
[20] Q. Chen and W. P. Risk, Electron. Lett. **18**, 1516 (1994).
[21] G. Rosenman, A. Skliar, M. Oron, and M. Katz, J. Phys. D **30**, 277 (1997).
[22] P. F. Fewster, J. Appl. Crystallogr. **22**, 64 (1989).
[23] P. F. Fewster, Appl. Surf. Sci. **50**, 9 (1991).
[24] P. F. Fewster, Appl. Phys. A: Solids Surf. **58**, 121 (1994).
[25] Z. W. Hu, P. A. Thomas, and J. Webjörn, J. Phys. D **28**, 189 (1995).
[26] Z. W. Hu, P. A. Thomas, and W. P. Risk, Phys. Rev. B **58**, 6074 (1998).
[27] Z. W. Hu, P. A. Thomas, and W. P. Risk, J. Phys. D **29**, 2696 (1996).
[28] P. A. Thomas and A. M. Glazer, J. Appl. Crystallogr. **24**, 968 (1991).
[29] Z. W. Hu, P. A. Thomas, M. C. Gupta, and W. P. Risk, Appl. Phys. Lett. **66**, 13 (1995).
[30] G. K. Wertheim, M. A. Butler, K. W. West, and D. N. E. Buchanan, Rev. Sci. Instrum. **45**, 1369 (1974).
[31] S. R. Andrews and R. A. Cowley, J. Phys. C **18**, 6427 (1985).
[32] I. K. Robinson, Phys. Rev. B **33**, 3830 (1986).
[33] A. Munkholm, S. Brennan, and E. C. Carr, J. Appl. Phys. **82**, 2944 (1997).
[34] B. W. Batterman and H. Cole, Rev. Mod. Phys. **36**, 681 (1964).
[35] M. E. Lines and A. M. Glass, *Principle and Applications of Ferroelectrics and Related Materials* (Clarendon, Oxford, 1977).
[36] M. M. Fejer, G. A. Magel, D. H. Jundt, and R. L. Byer, IEEE J. Quantum Electron. **28**, 2631 (1992).